Inner shelf response to Tropical Storm Floyd

Josh T. Kohut,[1] Scott M. Glenn,[1] and Jeffrey D. Paduan[2]

Received 20 October 2003; revised 23 May 2005; accepted 30 January 2006; published 27 September 2006.

[1] A continuously operated coastal observatory off the southern coast of New Jersey provides an opportunity to study both long-term trends and episodic events. On the evening of 16 September 1999, Tropical Storm Floyd moved up the New Jersey coast directly over the observatory. The response of the inner shelf is characterized using a depth-averaged (DA) and surface layer (SL) model in conjunction with direct observations. During the storm, the DA model was more representative of the observed response. While there was a peak in the near-inertial band of the depth average current, the response was not the typical clockwise ringing response seen in deepwater stratified regions. Instead the shallow, well-mixed inner shelf responded with an alongshore current oscillation balanced by the alongshore pressure gradient and bottom stress. The increased influence of bottom friction damps the typical inertial tail seen in deeper ocean responses and shortens the relaxation phase from several days to hours. Immediately following the storm, the surface layer model better represents the observed currents. It appears that the excessive rainfall associated with the storm and the resulting freshening of the inner shelf isolate the surface layer from the effect of bottom friction. The large waves and currents associated with the storm increase the potential for a sediment resuspension and transport event. Unlike the typical nor'easter in which the transport in this location is alongshore toward the south and onshore, the currents coinciding with the largest waves are alongshore toward the south but with an offshore component.

Citation: Kohut, J. T., S. M. Glenn, and J. D. Paduan (2006), Inner shelf response to Tropical Storm Floyd, *J. Geophys. Res.*, *111*, C09S91, doi:10.1029/2003JC002173.

1. Introduction

[2] Tropical storms and hurricanes force strong current responses over relatively short timescales. Since the generation and propagation of these storms is difficult to predict, most studies have utilized analytical and numerical models in conjunction with sparse observations to describe the structure of the current response. It has been shown that random wind forcing [*Kundu*, 1984] and fronts [*Kundu*, 1986; *Paduan et al.*, 1989] can generate a clockwise (CW) rotating near-inertial current. Most studies of wind forced responses associated with passing storms have focused on this frequency band. The typical deep ocean stratified response consists of a forced phase followed by an inertial tail that persists for several days [*Price et al.*, 1994]. This response has been described for several storms including Hurricane Allen in the gulf of Mexico [*Brooks*, 1983] and Hurricane Frederic off the coast of Alabama [*Shay and Elsberry*, 1987]. As is the case in the above examples, hurricanes are predominantly experienced in summer stratified waters. In the Mid-Atlantic Bight (MAB), Hurricane Belle forced two different responses on the outer and middle shelf [*Mayer et al.*, 1981]. The near-inertial middle shelf response lasted only 2 days compared to the longer response observed in the deeper water over the outer shelf. *Mayer et al.* [1981] identify friction as a possible contributor to this difference.

[3] Using the measured wind forcing as a boundary condition, a linear, inviscid model was used to predict the current response [*Shay et al.*, 1990; *Shay and Chang*, 1997]. During the storm, the stratified water column responded with a weak barotropic and strong baroclinic component. The baroclinic modes were independent of the free surface boundary condition and propagated energy out of the local surface layer within 4 inertial periods. A less energetic barotropic oscillation was added when the surface rigid lid condition was eased. *Keen and Glenn* [1999] found that the energy of the barotropic response propagated away from the storm as a Kelvin wave set up by the storm surge near the coast. *Keen and Glenn* [1995] modeled an inshore barotropic response where bottom friction increases shear in the full water column. Offshore the response remains a baroclinic two-layer response where bottom friction results in turning within the bottom Ekman layer [*Keen and Glenn*, 1995]. So over a shallow inner shelf, the relative importance of friction during storm forcing is increased.

[4] Both observations and models show that storm energy dissipates from the surface of a stratified ocean within several days and that the timescale of the dissipation can be shortened by friction. We test this mechanism for the shallow inner shelf during the passage of Tropical Storm Floyd. The local forcing and current response was captured

[1]Institute of Marine and Coastal Sciences, Rutgers–State University of New Jersey, New Brunswick, New Jersey, USA.
[2]Naval Postgraduate School, Monterey, California, USA.

0148-0227/06/2003JC002173

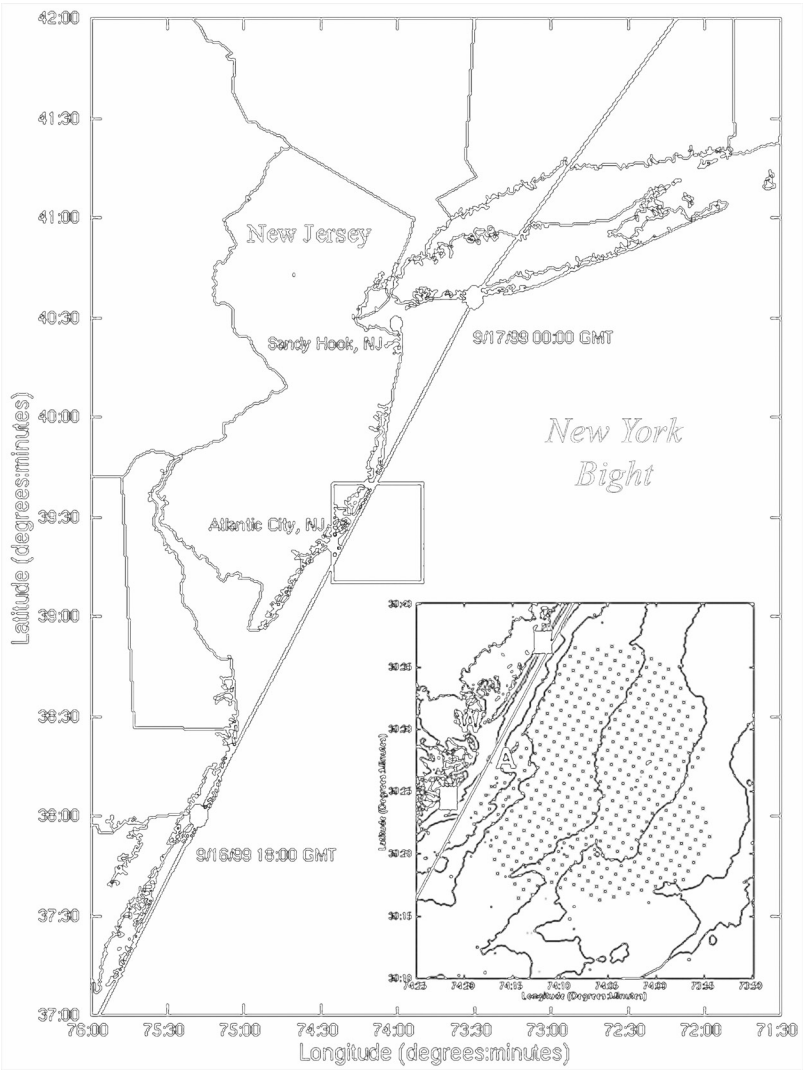

Figure 1. Storm track for Hurricane Floyd and the locations of the NOAA coastal sites in Atlantic City and Sandy Hook. The locations of the HF radar sites (squares), HF radar grid (asterisks), ADCP/CTD (A), and met station (W) are shown in the inset.

by a coastal ocean observatory located in Tuckerton New Jersey. Unlike the stratified and/or deep water seen in the responses outlined above, the shallow water column O(30 m) along the New Jersey inner shelf during Floyd was initially well mixed. The shallow water combined with the weak stratification increases the influence of bottom friction. While near-inertial currents have been observed within the study site, this response is typically seen during the summer months when the water column is stratified [*Chant*, 2001]. The observations are complimented with analytical models to characterize the current structure during and after the passing of Tropical Storm Floyd. Comparisons are drawn between this unstratified shallow water response and the deeper stratified, rotating response discussed above. Section 2 describes the instrumentation used in the study. An overview of the forcing associated with Tropical Storm Floyd is presented in section 3. Section 4 describes the current response to this forcing with observations and analytical models. Finally, section 5 presents implications to sediment transport and some concluding remarks.

2. Methods

2.1. Instrumentation

[5] The forcing and response to Tropical Storm Floyd was captured by several different components of an ocean observatory off the New Jersey coast (Figure 1). Remote systems including satellites and high-frequency (HF) radar provided coverage of ocean surface parameters such as sea surface temperature and surface velocity fields. The HF radar system uses two sites in Brant Beach and Brigantine, New Jersey (Figure 1) to generate hourly surface current maps [*Barrick et al.*, 1977; *Barrick and Lipa*, 1986]. All radial HF radar data were processed by the optimal techniques described by *Kohut and Glenn* [2003]. These techniques were demonstrated to produce the best comparison with concurrent in situ current meter data. The total vector

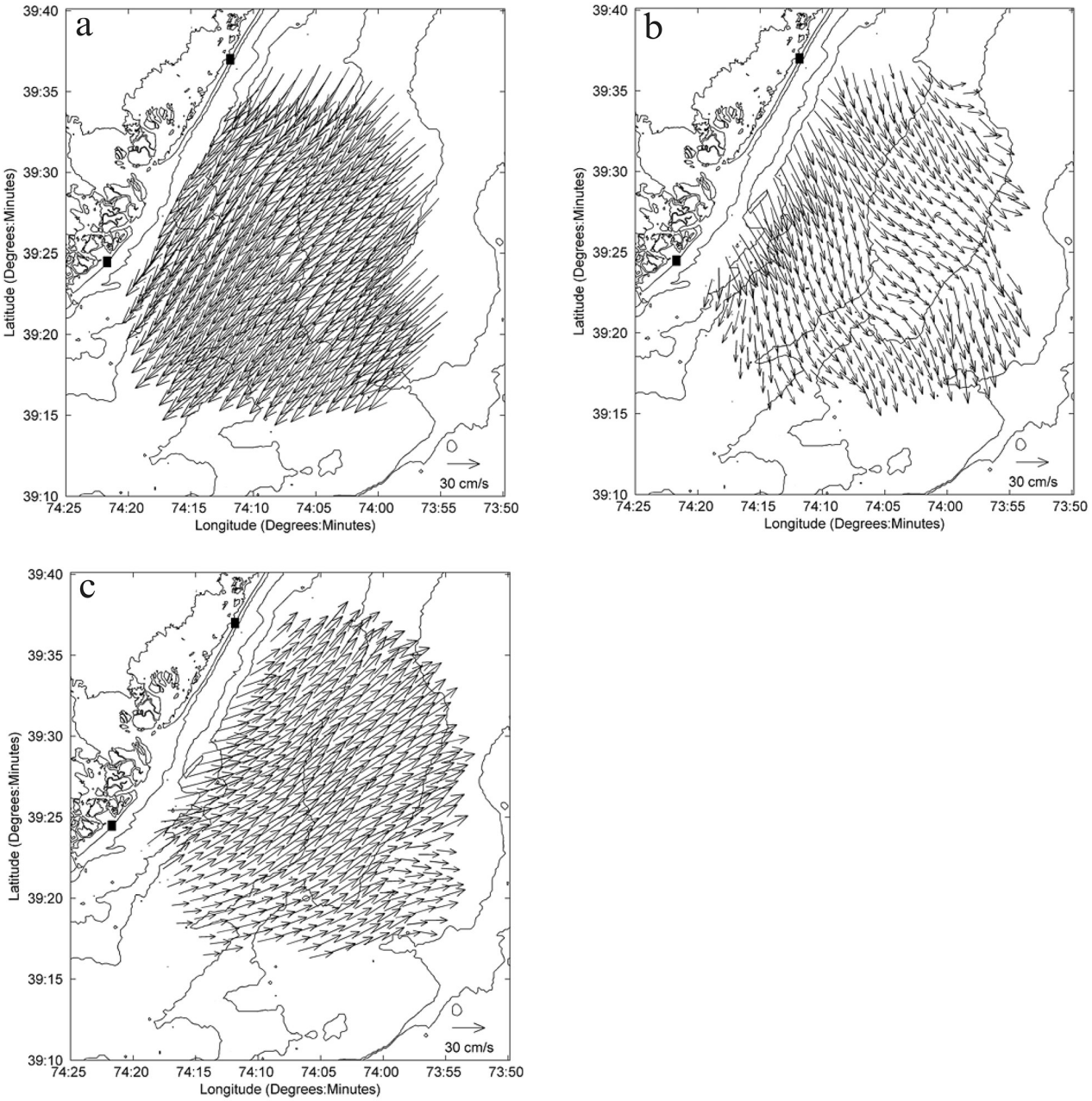

Figure 2. Detided surface current fields (a) before (YD 259.125), (b) at the peak significant wave height (YD 260.2083) of, (c) and following (YD 260.75) Tropical Storm Floyd.

HF radar grid stretches 40 km in the alongshore direction and about 30 km in the cross-shore direction (Figure 1). The Floyd data set is a subset of the annual record discussed by *Kohut et al.* [2004]. As discussed there, the time series data at each grid point were detided with a least squares fit of the dominant regional tidal constituents to a yearlong time series.

[6] Subsurface velocity was measured with a bottom-mounted ADCP located at the Long-term Ecosystem Observatory (LEO) [*Grassle et al.*, 1998; *Glenn et al.*, 2000a; *Schofield et al.*, 2001]. The ADCP is located about 5 km offshore in 12 m of water (Figure 1). The subsurface data were center averaged on the top of the hour and detided to match the sampling of the HF radar system. The depth-averaged flow discussed in this paper is an average of the ADCP data from 3 to 10 m and a surface measurement from an HF radar grid point closest to the ADCP. In addition to subsurface velocity, the LEO CTD provided time series data of bottom temperature, pressure and salinity. Using the time series of the measured temperature and salinity to calculate density and assuming a hydrostatic balance in the vertical, the sea level height was estimated at the LEO site. The sea level anomaly (SLA) is based on a 45 day mean. The measured SLA was corrected for atmospheric pressure and detided using the harmonic fit described above. SLA based on mean sea level (MSL) was also measured at two NOAA coastal sites in Sandy Hook (station 8531680) and Atlantic City (station 8534720), New Jersey (http://tidesandcurrents.noaa.gov/data_res.html) (Figure 1). These data were also

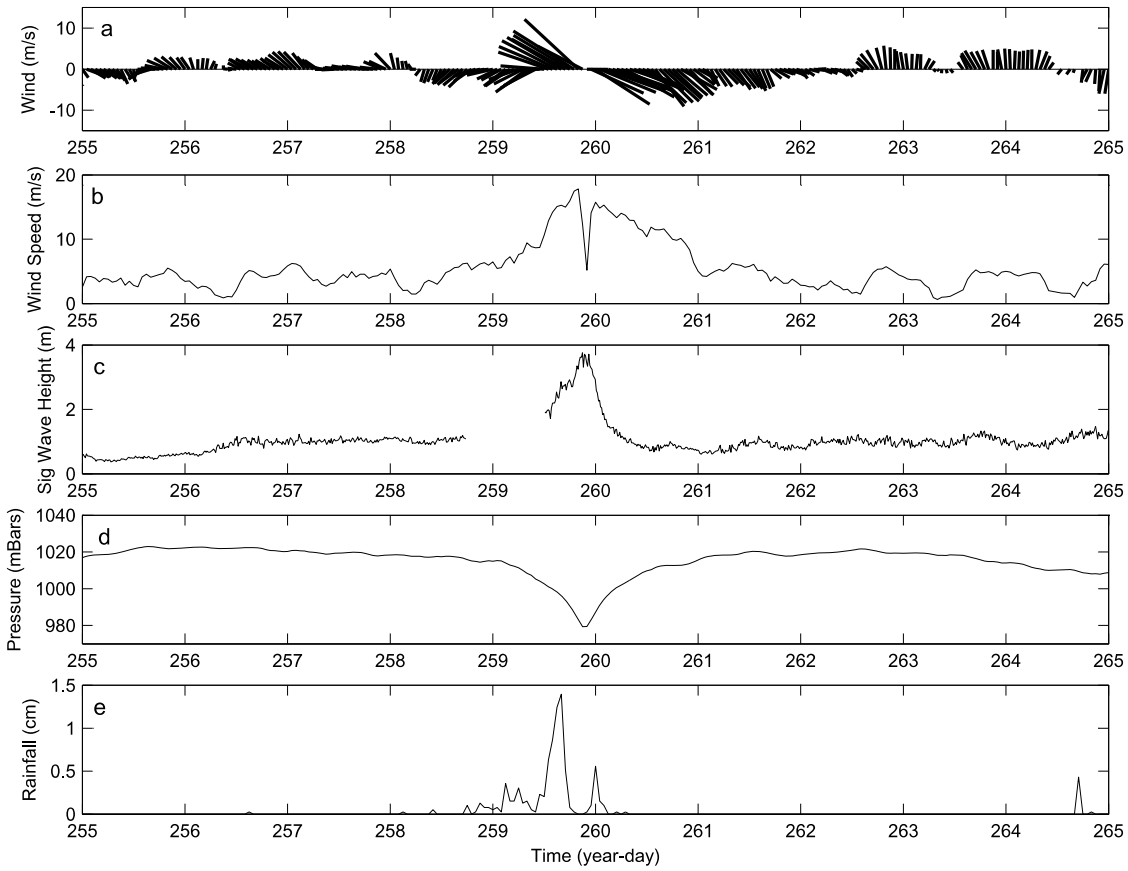

Figure 3. Time series of (a) wind velocity, (b) wind magnitude, (c) significant wave height, (d) barometric pressure, and (e) hourly Atlantic City precipitation surrounding Tropical Storm Floyd.

corrected for atmospheric pressure and detided. The meteorological data, measured at the Rutgers University Marine Field Station (Figure 1), includes time series data of atmospheric pressure, winds, temperature, and relative humidity.

2.2. Depth-Averaged Model

[7] *Fandry and Steedman* [1994] use the depth averaged shallow water equations to predict the nearshore response to a tropical storm propagating perpendicular and parallel to the coast. In both simulations, the pressure gradient is an important term in the balance [*Fandry and Steedman*, 1994]. The governing equations of the analytical model are

$$\frac{\partial u}{\partial t} = -g\frac{\partial \eta}{dx} + fv + \frac{\tau_{wx}}{\rho H} - \frac{\tau_{bx}}{\rho H} \tag{1}$$

$$\frac{\partial v}{\partial t} = -g\frac{\partial \eta}{dy} - fu + \frac{\tau_{wy}}{\rho H} - \frac{\tau_{by}}{\rho H} \tag{2}$$

where u and v are the depth-averaged cross-shore and alongshore velocity components, f is the local Coriolis parameter, η is the sea surface height, ρ is the water density, H is the water depth, τ_{wx} (τ_{bx}) is the wind stress (bottom stress) in the cross-shore direction, and τ_{wy} (τ_{by}) is the wind stress (bottom stress) in the alongshore direction. The nonlinear terms are not expected to be large for this forcing and response, and therefore are left out of equations (1) and (2) [*Shay and Elsberry*, 1987]. This is confirmed for this case by the observed surface current fields (Figure 2) in which the time varying flow is nearly parallel and uniform in space. The alongshore flow is about 40 cm/s toward the southwest before the storm, offshore at about 25 cm/s during the peak wave heights associated with the storm, and alongshore at about 30 cm/s toward the northeast after the storm (Figure 2). In the following analysis the acceleration (first term) and Coriolis force (third term) of equations (1) and (2) are calculated with the observed depth-averaged current.

2.2.1. Wind Stress

[8] The TOGA-COARE2.6 algorithm, modified for high wind, uses the wind velocity, air and sea temperatures, atmospheric pressure, and the relative humidity to predict the magnitude of the wind stress, τ_w [*Fairall et al.*, 1996]. All the atmospheric inputs are available from the meteorological tower. The direction of the wind stress is taken to be the observed wind direction.

2.2.2. Bottom Stress

[9] The magnitude of the bottom stress (τ_b) can be represented as

$$\tau_b = \rho u_*^2 \tag{3}$$

where u_* is the frictional velocity. Assuming a standard linear eddy viscosity, $K = \kappa u_* z$ and a constant stress layer, we get the following expression for u_*:

$$u_* = \frac{(u_2 - u_1)\kappa}{\ln\left(\frac{z_2}{z_1}\right)} \tag{4}$$

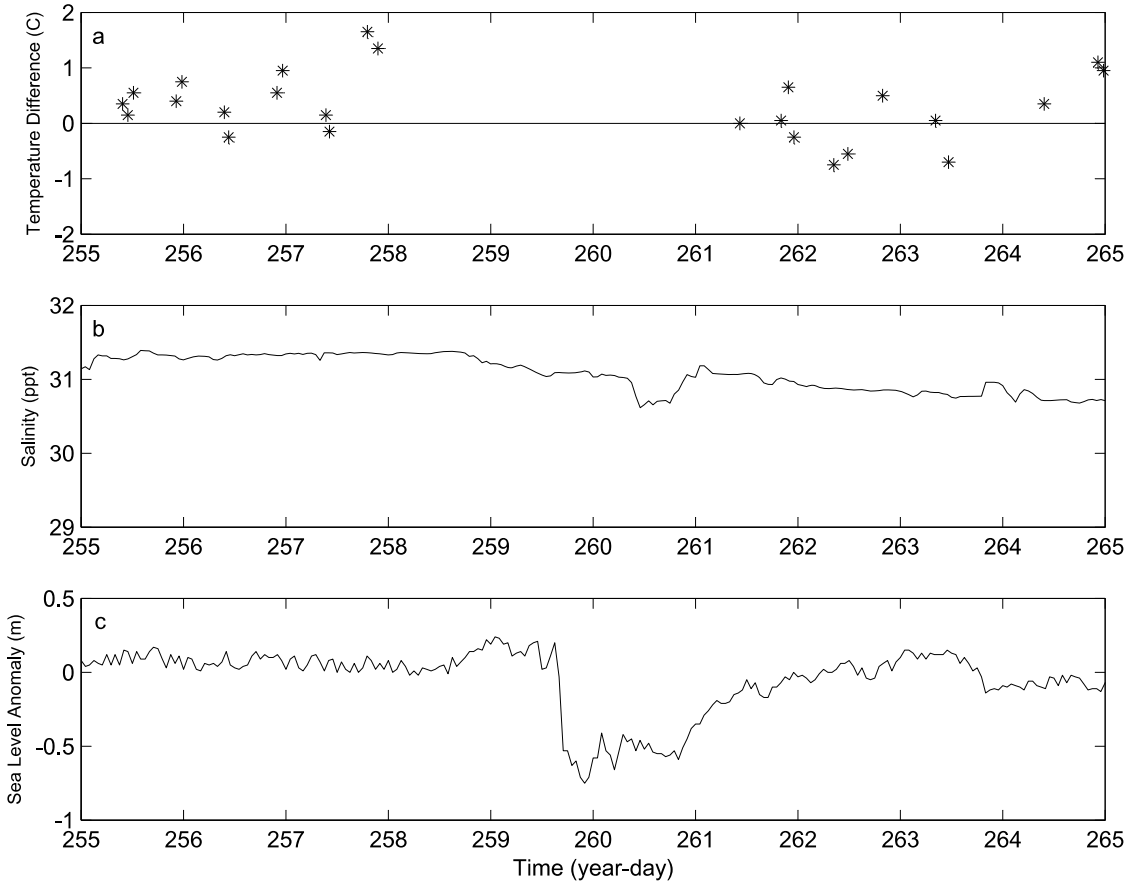

Figure 4. (a) Temperature gradient, (b) bottom salinity, and (c) sea level anomaly during the passage of Tropical Storm Floyd.

where $u_1[z_1]$ and $u_2[z_2]$ are the raw velocity (height above the seafloor) of the bottom two ADCP bins. *Forristall et al.* [1977] used this expression to calculate bottom stress during Tropical Storm Delia in the Gulf of Mexico. The frictional velocity, u_*, was then substituted into equation 3 to get the magnitude of the bottom stress, τ_b. The direction of the bottom stress is taken to be opposite the bottom current, u_1.

2.2.3. Pressure Gradient

[10] The sea surface slope, $\left(\frac{\partial \eta}{\partial x}, \frac{\partial \eta}{\partial y}\right)$, could not be measured directly at the offshore site. Instead it was inferred by requiring the measured terms and the unknown slopes in the model equations to balance. This inferred pressure gradient was compared to the sea level observations from the LEO and the NOAA coastal sites.

2.3. Surface Layer Model

[11] Immediately after the storm, there is evidence of a large freshwater input to the system (Figures 3 and 4). The freshwater potentially stratifies the water column changing the vertical structure of the current response. Both the magnitude and direction of the ADCP profiles show evidence of a two-layer system in which the surface layer is much less sheared than the bottom layer. Since the flow is stratified, the surface layer is separated from the bottom and no longer feels the effect of the bottom stress. For this reason, a second version of the model, more representative of a surface layer, was used. The model equations for the surface layer of this model are

$$\frac{\partial u_s}{\partial t} = -g\frac{\partial \eta}{dx} + fv_s + \frac{\tau_{wx}}{\rho H_s} \tag{5}$$

$$\frac{\partial v_s}{\partial t} = -g\frac{\partial \eta}{dy} - fu_s + \frac{\tau_{wy}}{\rho H_s} \tag{6}$$

where u_s and v_s are the surface layer averaged cross-shore and alongshore velocity components, f is the local Coriolis parameter, η is the sea surface height, ρ is the water density, H_s is the depth of the surface layer, and τ_{wx} (τ_{wy}) is the wind stress in the cross-shore (alongshore) direction. We assume the stress at the interface is small compared to the other terms due to stratification. For comparison, both the DA and surface layer (SL) models were run through the entire record. Using these models, the subtidal ocean response to the forcing both during, and immediately after the passing of Tropical Storm Floyd are discussed.

3. Forcing

[12] During the morning hours of 8 September 1999, Tropical Storm Floyd first formed about 1400 km east of the Leeward Islands. After two days, the storm strengthened

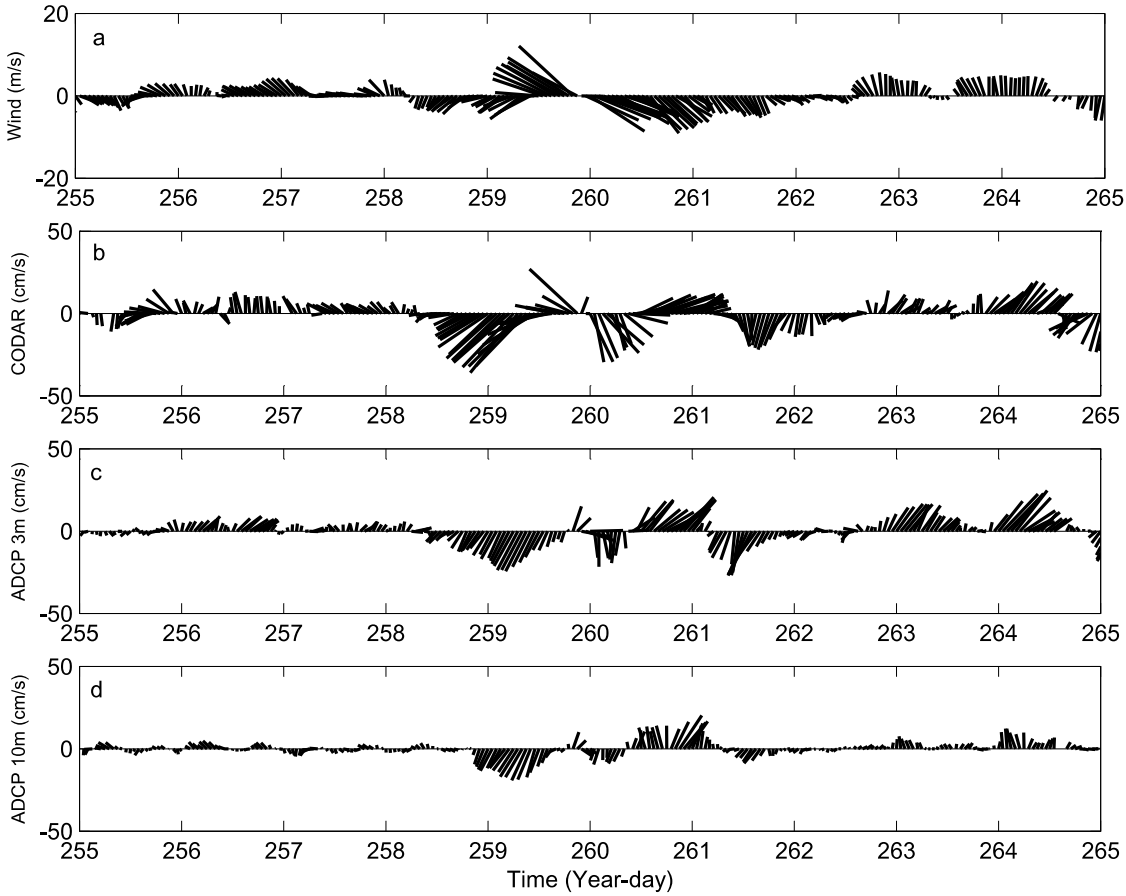

Figure 5. Time series of (a) wind velocity, (b) surface current, (c) current at 3 m depth, and (d) current at 10 m depth surrounding Tropical Storm Floyd.

to hurricane status and continued on a west/northwest track toward the eastern United States. Floyd's intensification fluctuated between category one and four on the Saffir/Simpson Hurricane Scale with sustained winds from 150 to 250 km/hr. The hurricane made landfall along the southern North Carolina coast at 0630 GMT on 16 September. At this time Floyd was a category 2 hurricane with sustained winds near 167 km/hr and a forward speed of about 28 km/hr. After landfall, the heavy rains caused extreme flooding as the storm weakened and accelerated toward the north/northeast. The effect of Floyd's rains and winds was seen at the mouth of the Chesapeake Bay with large freshwater outflow strong enough to reverse the flood tide [*Valle-Levinson et al.*, 2002]. Floyd was downgraded to a Tropical Storm just south of the study site at 1800 GMT on 16 September with sustained winds of 111 km/hr. The strong tropical storm continued moving toward the northeast along the New Jersey coast with a forward speed of about 54 km/hr (Figure 1). Wind data from the Rutgers meteorological station clearly shows the center of the storm arriving late on year day (YD) 259 (16 September) (Figure 3). The eye of the storm seen in the local winds and barometric pressure, passes through the study site at 2200 GMT on 16 September (YD 259.9167). Prior to the eye, the strong southeast winds peaked at 18 m/s (65 km/hr). Within the eye, the winds diminished to 5 m/s before 15 m/s northwest winds accompanied the second half of the storm. Throughout the period, the winds were predominately in the cross-shore direction. There was also locally heavy rainfall associated with the storm measured at Atlantic City, New Jersey (station 280311) (http://www.ncdc.noaa.gov) that peaked at 1.4 cm/hr prior to the storm eye (Figure 3e). This rainfall potentially increases the freshwater flux to the inner shelf after the storm.

[13] The inner shelf observatory focuses on the coastal ocean within the 30 m isobath. Within this shallow system, temperature gradients, calculated with surface satellite data and bottom CTD data, never exceed 2°C during and proceeding the storm (Figure 4a). Compared to the bottom water temperature, there is also a tendency for warmer water near the surface before the storm and cooler water near the surface after the storm, suggesting a freshening of the ocean surface after the storm. The bottom salinity minimum just after the storm also supports a freshwater pulse into the coastal ocean coincident with the storm rains (Figure 4b). Perhaps the strongest ocean signal associated with Floyd was seen in the sea surface height. A surge of 20 cm at the offshore site was followed by an 80 cm drop coincident with the eye of the storm (Figure 4c). This 80 cm drop is about 6% of the total water column. While the water column is initially well mixed prior to the storm, following the sea

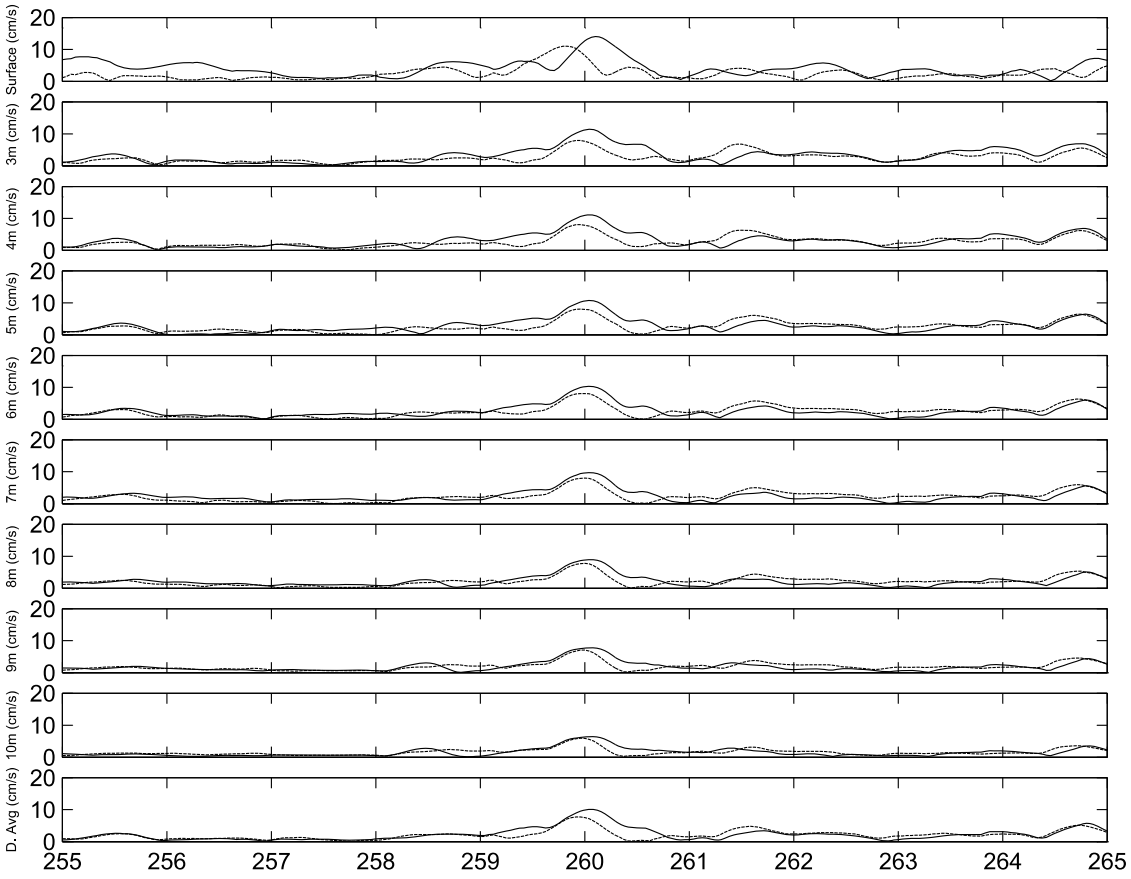

Figure 6. Vertical structure of the CW rotating (solid lines) and CCW rotating (dashed lines) components of the near-inertial response.

surface perturbation there is a freshwater pulse onto the inner shelf that potentially stratifies the system.

4. Response

4.1. Observed Response

[14] The vertical current structure several days before the storm was highly sheared (Figure 5). The stronger currents near the surface tend to follow the winds more closely than the weaker currents near the bottom. There is also a slight rotation to the left with depth. This rotation is representative of the typical vertical structure seen throughout the fall of 1999 [*Kohut et al.*, 2004]. As the storm approaches, this climatology breaks down and the currents increase and become more uniform with depth (Figure 5). Even though the wind forcing is primarily in the cross-shore direction (NW or SE), the depth-independent current response is predominately alongshore (NE or SW). Within 48 hours of the storm onset, the episodic response is replaced by the seasonal structure observed before the storm.

[15] Like the storm response papers outlined in the introduction, we looked at the spatial and temporal structure of the near-inertial current response. The near inertial component of the flow was obtained using a least squares fit to the detided time series. The local inertial period of 18.87 hours was fit to the data using a 1.5 day moving window. This technique has been used in previous dynamical studies and is the mathematical equivalent to complex demodulation [*Chant*, 2001].

[16] The near-inertial band has a peak during the storm, between YD 259 and YD 261 (Figure 6). There is very little vertical structure in the band except for slightly weaker amplitudes near the bottom. The equal amplitude of the clockwise and counterclockwise rotating components indicates that, like the forcing and unlike the deepwater response discussed in the introduction, the ocean response is rectilinear. Throughout the duration of the storm, the kinetic energy within the near-inertial band is 68% of the kinetic energy of the subtidal, depth-averaged currents.

[17] Spatial maps of the near-inertial motion show that this rectilinear response is oriented in the alongshore direction (Figure 7). At one half inertial period before the storm, the strongest response is seen in the shallower water near the coast. There is a slight 5° advance in phase between the center and northern edges of the field with the center leading the northern edge. The phase propagation speed can be approximated using the local inertial period of 18.87 hours, the 5° phase shift, and the alongshore distance of approximately 20 km. The resulting phase propagation speed of 75 km/hr is consistent with the 54 km/hr translation speed estimate for the storm. When the eye is directly over the study site, the response is in phase and reaches its peak amplitude over the entire field. Within half an inertial period after the storm, the response, still in phase, has significantly decreased across the field. Throughout the

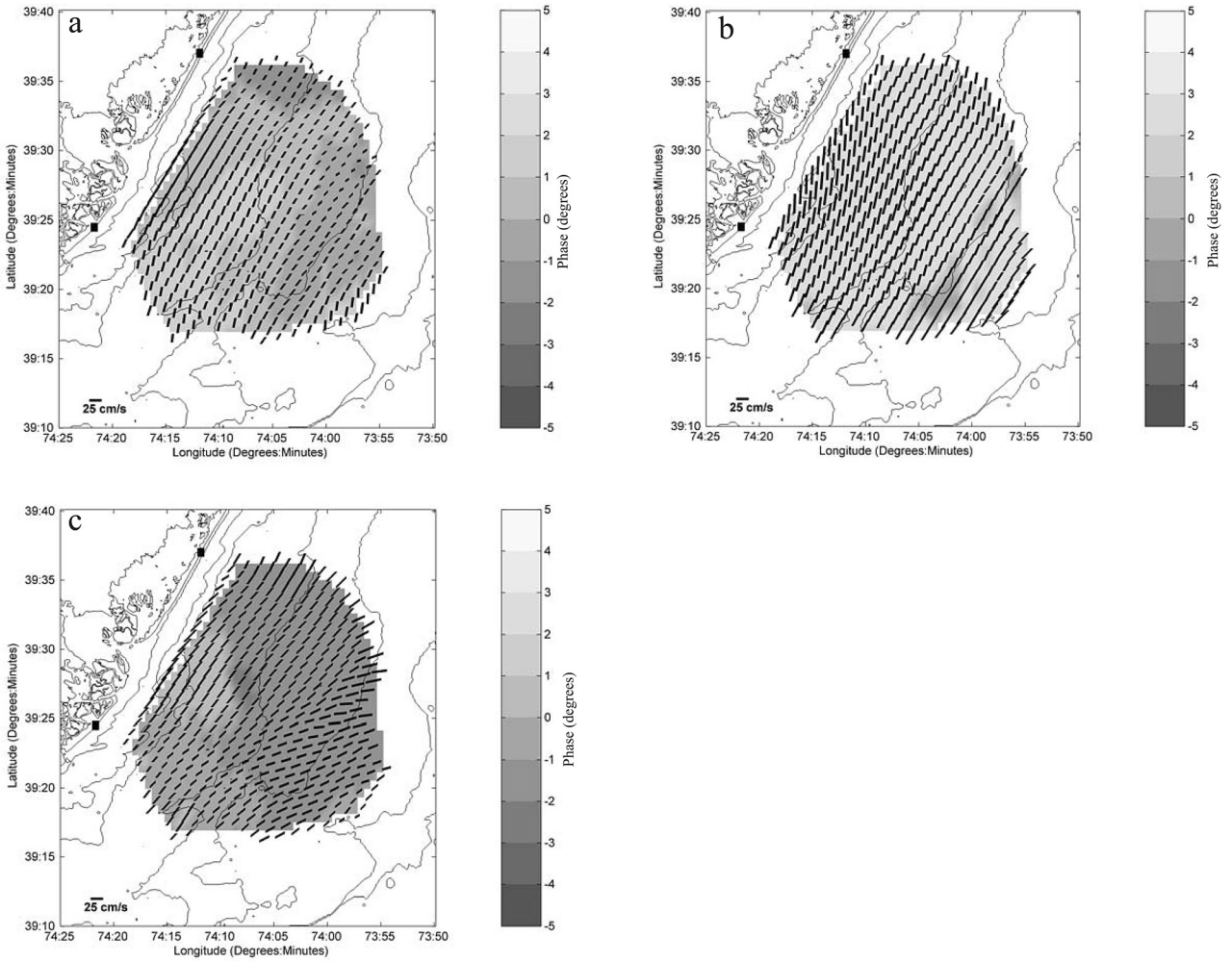

Figure 7. Amplitude, orientation, and phase of the near-inertial ellipses (a) one half inertial period before, (b) during, and (c) one half inertial period after the passing of Tropical Storm Floyd.

entire event, the near-inertial response is nearly uniform across the HF radar field and peaks with the storm.

[18] The near-inertial band of the subsurface response is also rectilinear with a mean eccentricity on the order of 10^{-3}, equivalent to an aspect ratio 1000 to 1 between the major and minor axis. Half an inertial period before the eye, the amplitudes are relatively weak with an 8 cm/s maximum near the surface (Figure 8). There is a slight rotation to the left with depth, however, the ellipses are generally oriented along the coast. Similar to the surface response the amplitudes peak near the center of the eye with amplitudes reaching 18 cm/s near the surface and 12 cm/s near the bottom. Once again, the ellipses are oriented with the coast and in phase throughout the water column.

[19] The near-inertial response observed here is not a typical CW rotating response. Unlike the deeper more stratified responses, the currents here slosh back and forth in the alongshore direction. The energy observed in the near-inertial band is not the CW "ringing" response observed in a deeper, more stratified water column, but rather a consequence of the timescale of the storm forcing. During the deeper more stratified response, the near-inertial energy occurs after the storm and last several days. In this shallow well-mixed response the near-inertial energy peaks during the direct forcing and quickly dissipates following the storm.

[20] The remainder of the paper will focus on the short-lived, rectilinear response using the DA and SL models. Since the larger-scale response is relatively uniform in space, the nearshore response during the direct storm forcing and immediate response, will utilize the ADCP and CODAR derived depth-averaged and surface layer flows. The analysis is described for two periods, the first during the storm and the second immediately after. These time periods were chosen based on the storm characteristics. Assuming a propagation speed of 54 km/hr and an approximate storm radius on the order of 400 km, the study site was directly impacted by the storm for approximately 15 hours. So the first time period was chosen to be 15 hours long, centered at the passing of the eye over the offshore site. The period following the storm was chosen to begin immediately after the storm forcing and continue for 15 hours. On the basis the representative vertical current structure following the storm (Figure 9), the depth of the surface layer, H_s, in the SL model is taken to be 8 m. Since this response is not a typical rotating, ringing response and

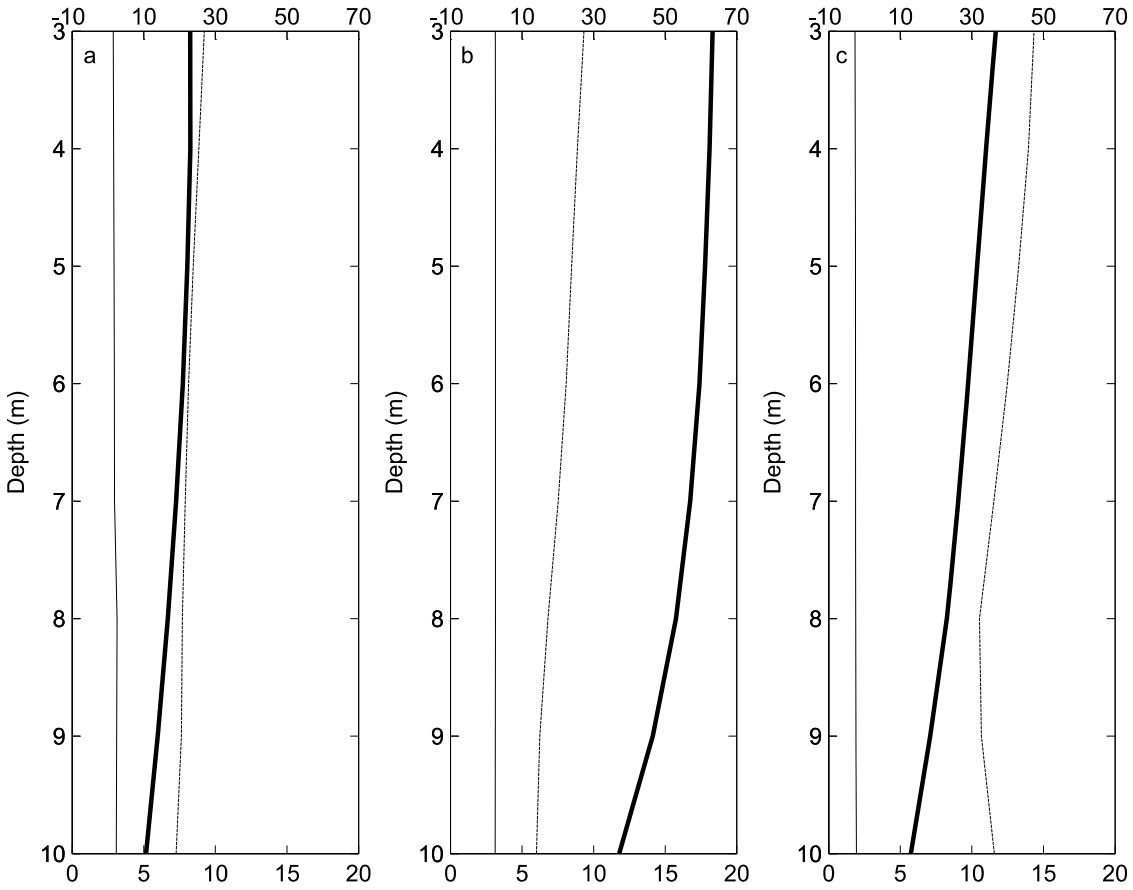

Figure 8. Magnitude (thick lines), inclination (dashed lines), and phase (thin lines) of the near-inertial rectilinear response (a) one half inertial period before, (b) during, and (c) one half inertial period after the passing of Tropical Storm Floyd.

the energy in the near-inertial band is 68% of the total kinetic energy, the following analysis describes the entire subtidal ocean response of the storm. The model data will be presented within these time periods, during and after the direct storm forcing.

4.2. Modeled Response During the Storm

[21] As Floyd approaches the study site, the current response accelerates up and down the coast with a weak cross-shore component. The cross-shore balance of the DA model is between the onshore wind stress and the inferred pressure gradient (Figure 10b). In the eye, the onshore winds decrease and the cross-shore current accelerates offshore with the pressure gradient. Bottom friction then increases to balance the large inferred pressure gradient associated with the storm surge. The direction of the spike indicates that the surge is larger near the coast than offshore at the ADCP/CTD. Immediately after the eye, the sea surface flattens in the cross-shore direction and the weak offshore currents are again balanced primarily by the inferred pressure gradient and the wind stress. With the SL model, the cross-shore velocity of the surface layer is very similar to that seen in the DA model (Figure 10). There is initially a weak onshore flow followed by an offshore flow coincident with the eye of the storm. Since the surface layer doesn't feel the effect of bottom stress, the inferred pressure gradient is balanced by the wind stress. This results in a sloping sea surface that changes sign with the changing winds on either side of the storm eye.

[22] Since the pressure gradient term in both models is inferred to balance the measured terms, each inferred pressure gradient was compared to a measured sea surface slope to determine which model better represents the true force balance. Available coastal sites (Figure 1) were chosen for the alongshore and cross-shore components. The storm propagates very quickly through the study area, about 50 km/hr, covering the 15 km alongshore distance between the Atlantic City site and the LEO-15 site in 18 min. Therefore the sea level difference measured between these two sites is assumed to be representative of the cross-shore pressure gradient particular to the storm. Both the inferred DA model and measured slopes tilt up toward the coast for the duration of the storm, indicating a larger storm surge near the coast (Figure 11a). The SL model slope, on the other hand, changes sign as the storm moves through the region. Even though the measured surge is an order of magnitude larger than that seen in the DA model, the slope is always negative. The discrepancy between the magnitude of the measured and the DA model slopes indicates that nearshore processes may amplify the surge near the coast. This is consistent with long wave theory over irregular-shaped basins that suggests that the cross-shore slope of the storm surge is steeper over shallower water [*Dean and Dalrymple*, 1991]. *Dean and Dalrymple* [1991] go on to

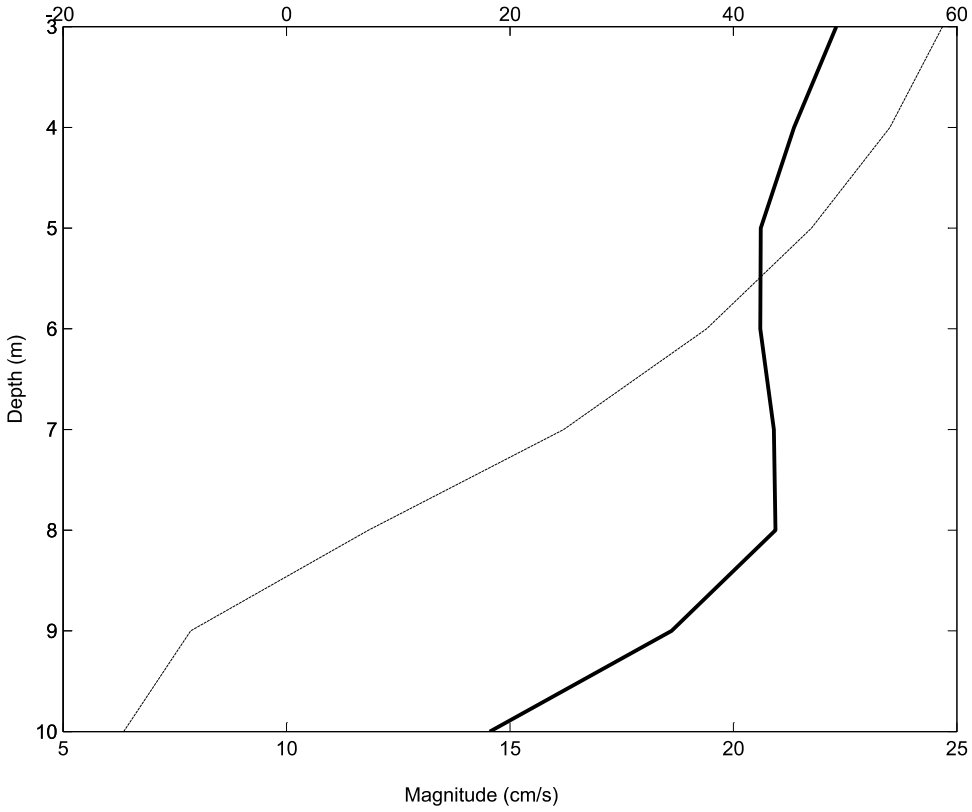

Figure 9. Vertical structure of the magnitude (solid line) and direction (dashed line) of the two-layer flow observed after Floyd.

show that for a given bottom stress, the steeper the bottom slope, the steeper the storm surge near the coast. Therefore most of the measured 2.5 m rise observed between the Atlantic City site and the offshore site could occur very close to shore. The 25 cm rise seen in the DA model is likely more representative of the slope acting on the depth-averaged current in the deeper 12 m water column. A time series of the SLA measured at both Atlantic City and the offshore site clearly illustrates the larger surge near the coast (Figure 12). Since the slope of the SL model changes sign during the storm and does not maintain the slope seen in the DA model, it appears that the DA model is more on track with the observations during this segment.

[23] In the alongshore direction, there are three current events associated with the storm. The important terms in the DA model are a combination of the bottom stress, pressure gradient and acceleration (Figure 13). As the storm approaches, the surge south of the study site tilts the sea surface down toward the north. This is seen in the term balance as an acceleration to the north followed by a balance between the pressure gradient and bottom stress. Immediately after the storm, the surge moves through the site and the pressure gradient changes sign. This event starts as acceleration toward the south followed again by a balance between the pressure gradient and bottom stress. After the storm has left the area there is another acceleration toward the south that once again is followed by a balance between the pressure gradient and bottom stress. This small event is correlated with the large rainfall associated with the storm (Figure 3e) and the salinity minimum observed offshore near the bottom (Figure 4b). The three current events are also seen in the mean surface layer flow of the SL model, however the force balance of this model shows an acceleration driven by the pressure gradient term. Since there is no bottom stress in this model, the influence of the wind stress on the overall balance is increased (Figure 13d).

[24] Once again the inferred pressure gradient of each model was compared to a measured sea surface slope. For the alongshore component, the slope was calculated between the Sandy Hook and the Atlantic City sites. In the measured, DA model, and SL model there is evidence of all three events (Figure 11). The largest is seen during the second event associated with a surge north of the site. While there is evidence of all three events in both the DA and SL inferred pressure gradients, the second event is much smaller in the SL model (Figure 11b). Both the measured and DA model slopes are on the order of 10 cm over 10 km. There is a 1 hour time offset in which the measured slope leads the DA modeled slope. This offset between the 2 peaks could be due to differences that occur when comparing a sea level difference measured across 115 km (distance between the Atlantic City and Sandy Hook sites) to a predicted gradient based on observations collected at a single point 5 km offshore. The magnitude of the three event structure is similar in both the observations and the DA model. The SL model, however, underestimates the slope, especially that associated with the second event. Once again it appears that the DA model is more on track for the period during the storm. Both the cross-shore and alongshore components of the DA model indicate the

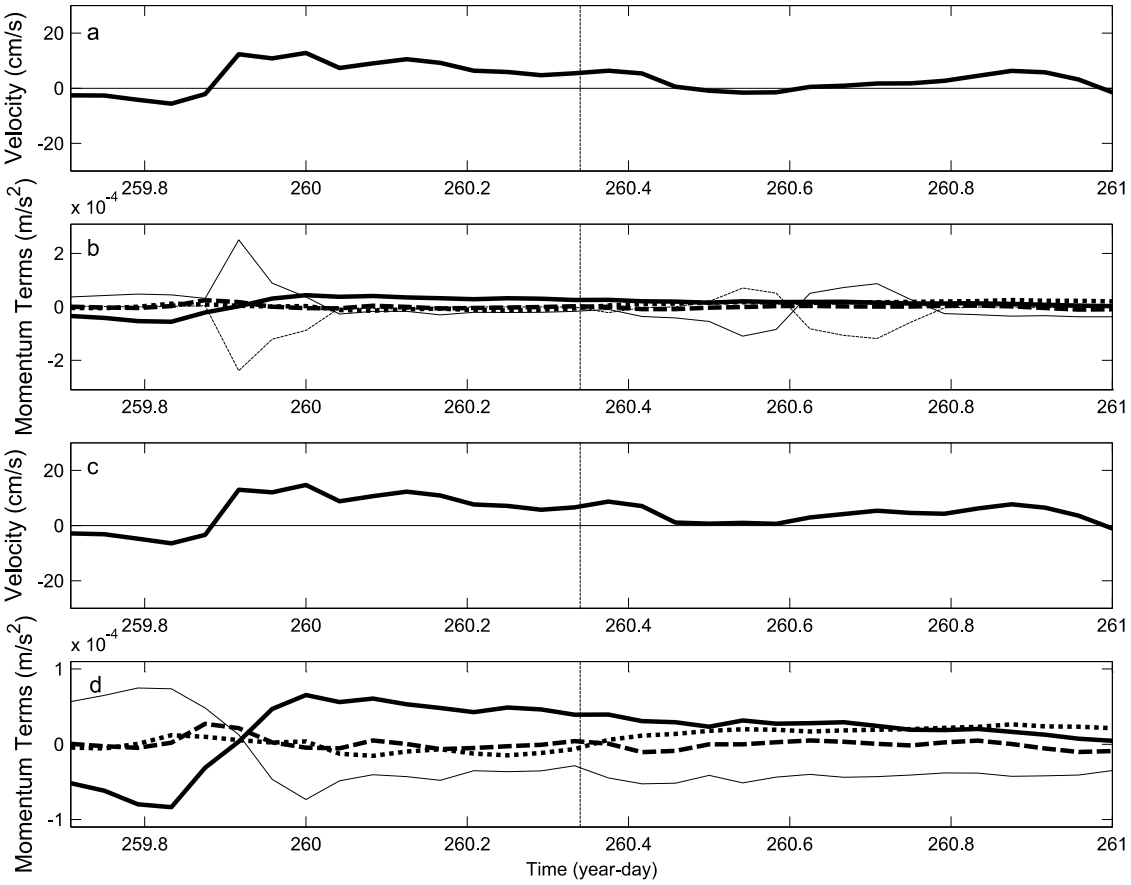

Figure 10. Cross-shore (a) depth-averaged velocity, (b) depth-averaged momentum balance, including the acceleration (thick dashed line), Coriolis (dotted line), wind stress (thick solid line), bottom stress (thin dashed line), and pressure gradient (thin line) terms, (c) surface layer velocity, (d) surface layer momentum balance, including the acceleration (thick dashed line), Coriolis (dotted line), wind stress (thick solid line), and pressure gradient (thin solid line) terms. The vertical dashed line separates the data into the during and after storm regimes.

currents associated with the storm slosh back and forth with the pressure gradient.

4.3. Modeled Response After the Storm

[25] After the storm, freshwater from the strong rains associated with Floyd potentially stratifies the water column. The cross-shore component of the SL model has a steady cross-shore surface layer flow in which the pressure gradient balances both the wind stress and Coriolis (Figure 10). The DA model is a multiterm balance between the wind stress, pressure gradient, Coriolis, and bottom stress. The exception to this multiterm balance is between YD 260.4 and 260.8 when the balance is dominated by two terms, the pressure gradient and bottom stress (Figure 10). During this time, the sea surface slope changes sign several times to balance the bottom stress. This oscillation is not seen in either the measured or SL model slopes (Figure 11). This fluctuation, seen only in the DA model, is due to an apparent overprediction of the influence of bottom stress on the surface currents. The large bottom stress requires that the sea surface slope compensate to keep the model in balance.

[26] Similarly in the alongshore direction, the DA model is predominately a two-term balance between the pressure gradient and the bottom stress terms (Figure 13). In the SL model there is a multiterm balance between acceleration, pressure gradient, Coriolis, and wind stress. The resulting pressure gradient is much smaller than that seen in the DA model (Figure 13). The measured alongshore pressure gradient between the two coastal sites in Sandy Hook and Atlantic City agrees much closer with the SL model slope than that seen in the DA model (Figure 11b).

[27] In both the alongshore and cross-shore direction, the bottom stress term in the DA model leads to an overprediction of the sea-surface slope. On the basis of comparisons to the observed sea surface slopes, it appears that the SL model, where bottom stress does not affect the surface layer, better represents the upper ocean force balance immediately following the storm. Even though the water column is largely isothermal (Figure 4a), the large input of freshwater by the storm into the system likely stratifies the fluid. Since the vertical temperature gradient after the storm is negative (Figure 4a), the water column must be composed of a cold, fresher layer over a warm, more saline layer. The

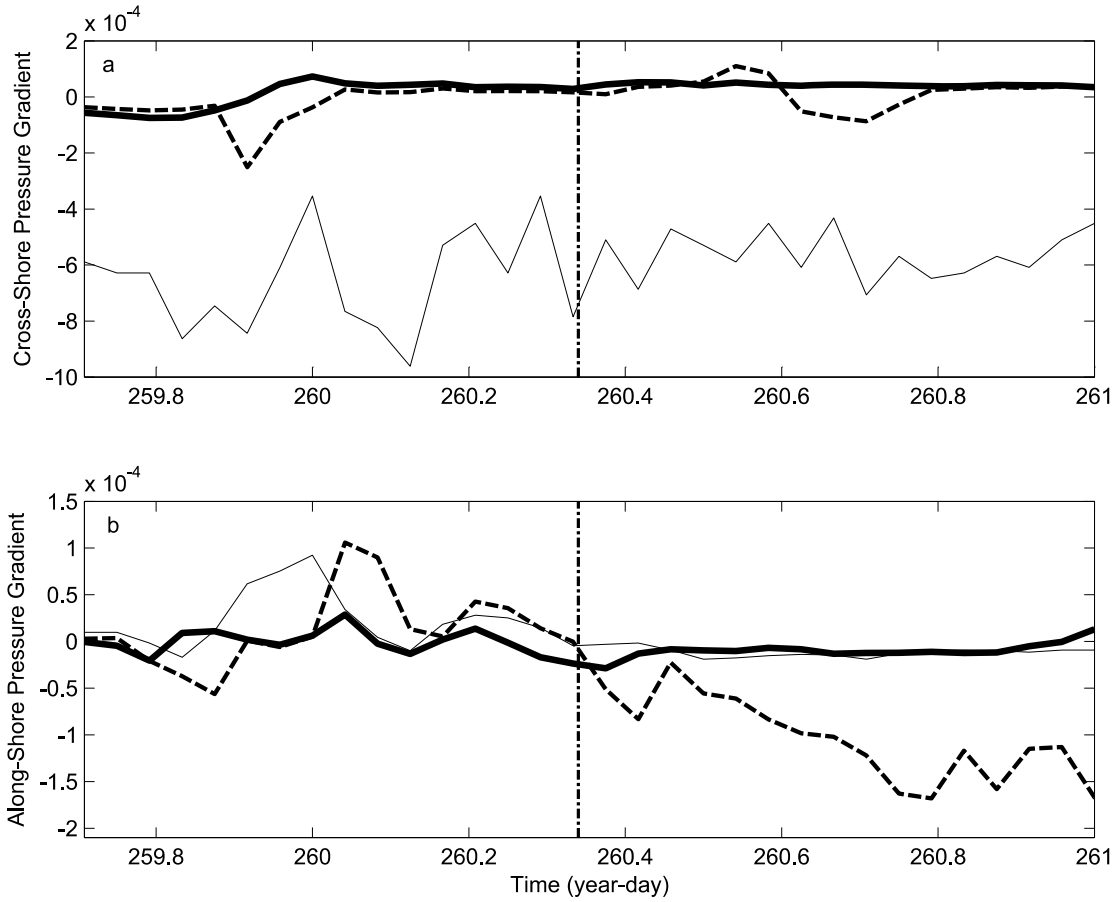

Figure 11. (a) Cross-shore and (b) Alongshore components of the measured (thin lines), inferred depth averaged (dashed lines), and inferred surface layer (thick lines) pressure gradient. The vertical dashed line separates the data into the during and after storm regimes.

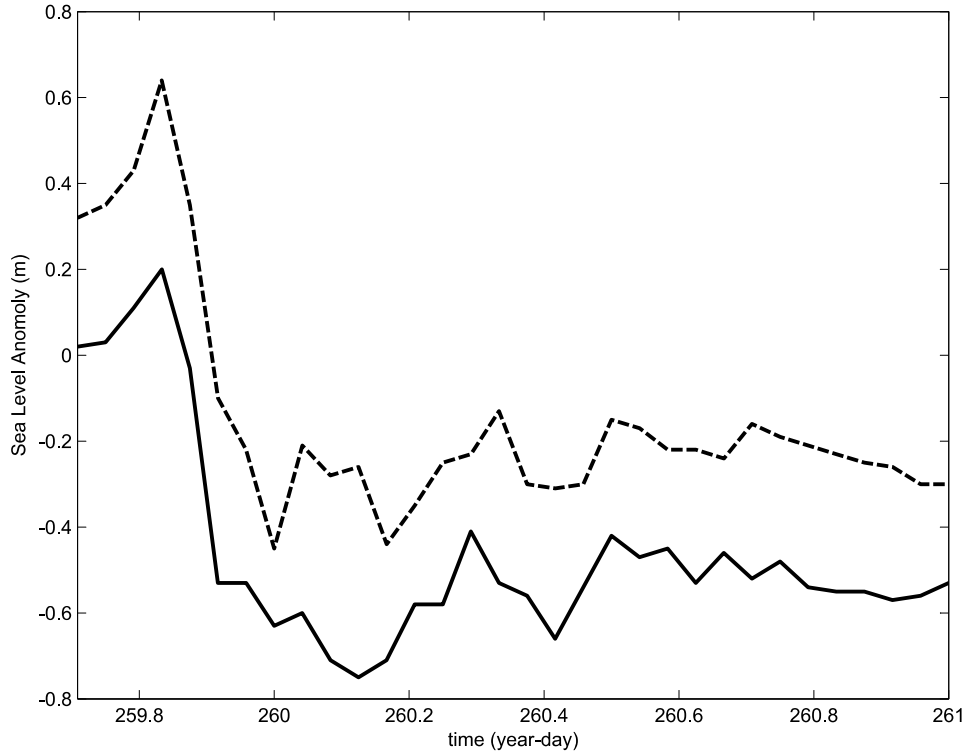

Figure 12. SLA measured at Atlantic City (dashed line) and the offshore node (solid line).

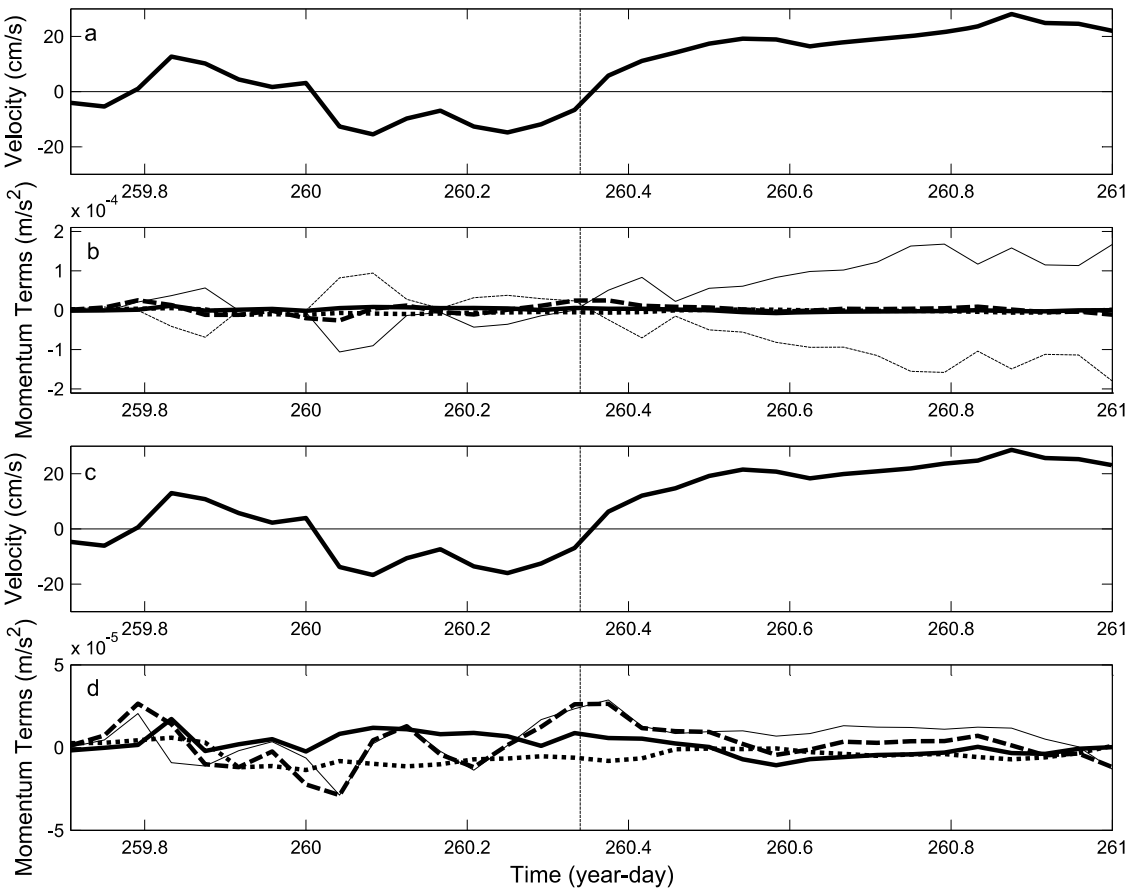

Figure 13. Alongshore (a) depth-averaged velocity, (b) depth-averaged momentum balance, including the acceleration (thick dashed line), Coriolis (dotted line), wind stress (thick solid line), bottom stress (thin dashed line), and pressure gradient (thin solid line) terms, (c) surface layer velocity, (d) surface layer momentum balance, including the acceleration (thick dashed line), Coriolis (dotted line), wind stress (thick solid line), and pressure gradient (thin solid line) terms. The vertical dashed line separates the data into the during and after storm regimes.

SL model and measured alongshore pressure gradients indicate a rise of about 1 cm over 10 km. The stratification induced by the large rain event appears to isolate the surface layer from the effect of bottom friction in the observed response. The structure of the current response after the storm is more representative of a two-layer flow in which the acceleration of the surface layer is balanced by the alongshore pressure gradient.

4.4. Energy Flux of the Response

[28] The energy associated with the storm response differentiates the shallow water response from the deep water responses outlined in the introduction. In deep water, the energy put into the system by the passing storm was predominately in the near-inertial band and dissipates very slowly over several days. This is referred to as the "relaxation stage" of the response by *Price et al.* [1994]. This relaxation stage typically lasts for 5 to 10 days. For the specific case of Floyd and the shallow inner shelf, the entire event is much shorter. The energy put into the system dissipates much faster.

[29] The energy pathways associated with Tropical Storm Floyd were identified with a work equation based on the DA model during the initial time period in which it appears to be more representative. The work done by each term was calculated by multiplying equations 1 and 2 by velocity so that

$$\frac{\partial KE_x}{\partial t} = -g\frac{\partial \eta}{dx} \bullet u + fv \bullet u + \frac{\tau_{wx}}{\rho H} \bullet u - \frac{\tau_{bx}}{\rho H} \bullet u \qquad (7)$$

$$\frac{\partial KE_y}{\partial t} = -g\frac{\partial \eta}{dy} \bullet v - fu \bullet v + \frac{\tau_{wy}}{\rho H} \bullet v - \frac{\tau_{by}}{\rho H} \bullet v \qquad (8)$$

Each term on the right side of the equations is the work done by the respective term in equations 1 and 2. The work done by the wind and bottom friction was then compared to the change in kinetic energy (KE) of the entire system with time. The following discussion focuses on the energy input and dissipation particular to the storm.

[30] The kinetic energy associated with the storm increases sharply around YD 259.8 as the storm approaches (Figure 14a). Throughout the storm there are three distinct peaks in the kinetic energy. Preceding each of these peaks is an increase in the total work (term 1 in equations (7) and (8)) (Figures 14b and 14c). Since the peaks in the work done by the wind do not appear to coincide with these energy

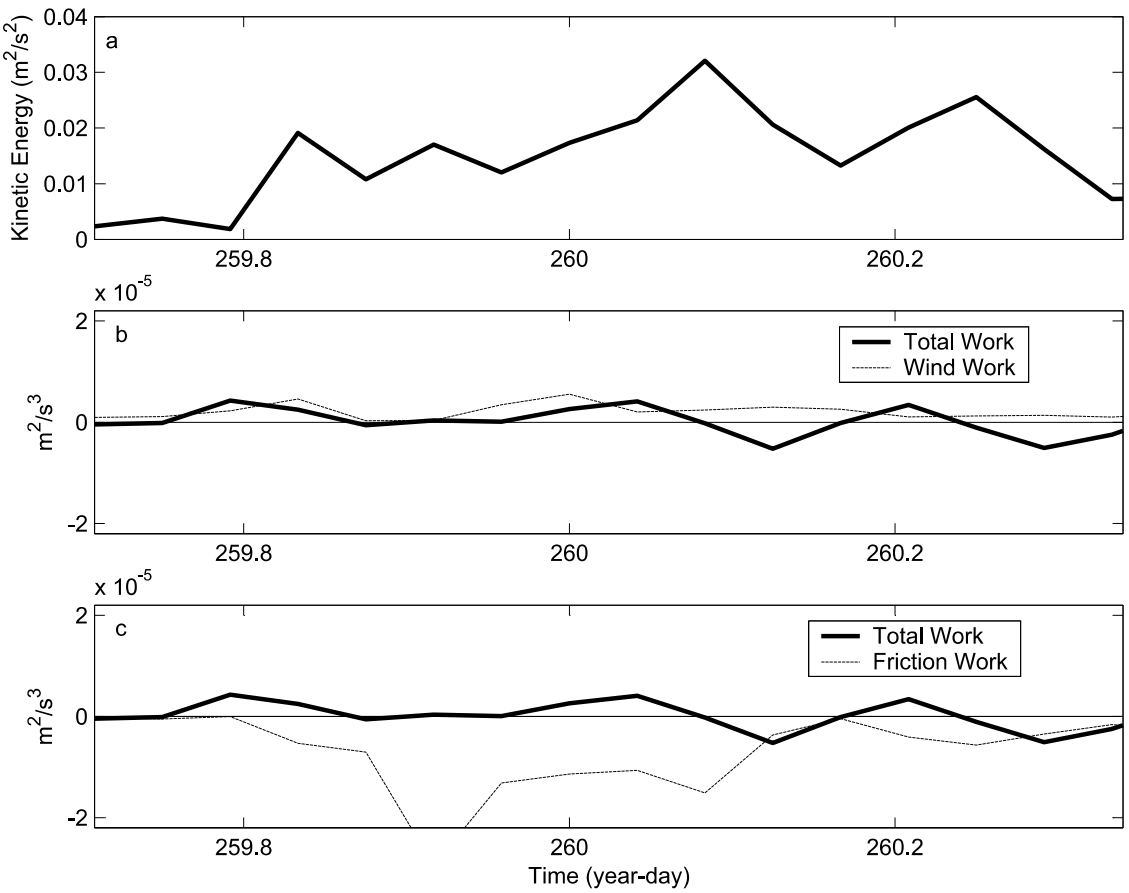

Figure 14. Total (a) kinetic energy, (b) work done by the wind, and (c) work done by bottom friction. The total work is quantified as the change in kinetic energy.

peaks, the wind does not appear to contribute significantly to the net increase in the total work. These three peaks are instead associated with the oscillating sea surface slope. With each increase in the kinetic energy there is an increase in the magnitude of the work done by the bottom friction term. So any energy added to the system by the oscillating pressure gradient is quickly dissipated by bottom friction. A closer look at the individual components of the energy equations shows a clear interaction between the cross-shore and alongshore components of the total work.

4.4.1. Cross-Shore Energy

[31] The kinetic energy of the cross-shore current component is very weak throughout most of the study period except for the peak coincident with the eye of the storm (Figure 15a). As the storm approaches, the cross-shore wind adds energy to the system without changing the kinetic energy (Figure 15b). Instead the wind work builds up the potential energy of the system in the form of a pressure gradient. It is not until the wind dies in the storm eye that this potential energy is turned into kinetic. Following the peak in kinetic energy, the bottom friction work peaks, quickly dissipating the energy added by the wind (Figure 15c).

4.4.2. Alongshore Energy

[32] The alongshore currents are more energetic than that seen in the cross-shore balance (Figure 16a). Since the wind forcing during the storm is predominately in the cross-shore direction, the work done by the alongshore wind stress is very small throughout the study period (Figure 16b). During the storm, kinetic energy is added and taken away from the system with each sea level oscillation observed and discussed in the previous section. Like the cross-shore direction, a peak in bottom friction work follows each input of kinetic energy so that the energy put into the system by the oscillating pressure gradient is quickly taken out by bottom friction (Figure 16c).

[33] By separating the energy budget into the cross-shore and alongshore directions, the contribution of the cross-shore winds to the oscillating sea level is more evident. The storm winds set up an alongshore pressure gradient that moves up the coast with the storm. The energy associated with the moving pressure gradient is quickly diminished by bottom friction. In this shallow well-mixed ocean there is no time for the energy to propagate away before the bottom stress dissipates all the energy. For this reason, the response to this storm is shorter relative to the modeled and observed responses of a deeper more strongly stratified ocean.

5. Conclusions

[34] The two analytical models chosen for this study provide insight on the apparent force balances responsible for the observed response to Tropical Storm Floyd. While

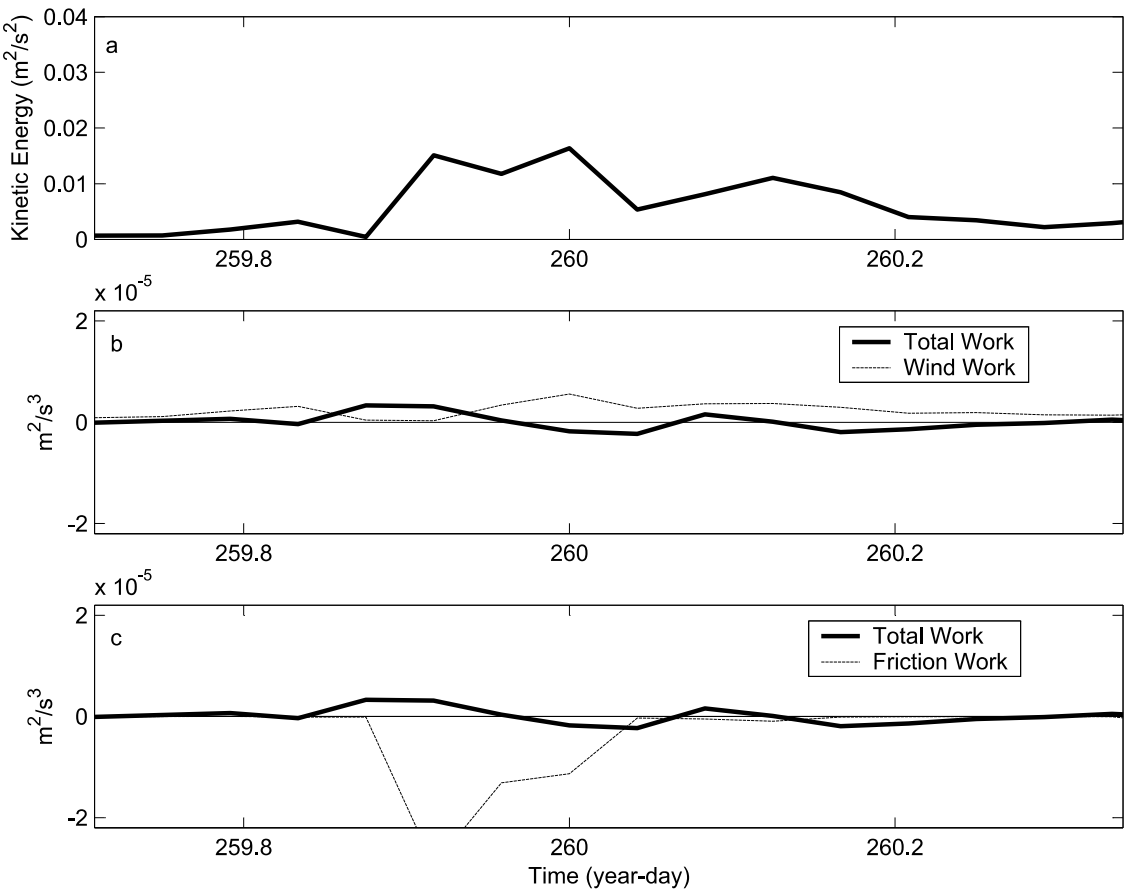

Figure 15. Cross-shore (a) kinetic energy, (b) work done by the wind, and (c) work done by bottom friction. The total work is quantified as the change in kinetic energy (equation (7)).

there were no direct measurements of the local pressure gradient term, the DA model pressure gradient was more consistent with the sign of the available observations during the storm and the SL model was more consistent after the storm. During the storm forcing, the dominant balance was between the pressure gradient and the bottom stress, driving an alongshore current that switched from northward to southward (Figure 2). After the storm, freshwater stratifies the system and the dominant balance of the surface layer is between the acceleration and local wind stress. In the future, better estimates of sea surface slopes from arrays of bottom pressure sensors could help to describe the response in more detail.

[35] Floyd also generated large waves as it propagated up the coast so there is potential for a large sediment resuspension and transport event. The largest waves observed at the offshore LEO site coincide with the southward current event immediately following the passage of the storm eye (Figure 17). With equivalent bottom wave orbital velocities [*Styles and Glenn*, 2002] on the order of 80–100 cm/s and depth averaged currents on the order of 20 cm/s toward the south, the integrated sediment transport during the storm will be to the south and offshore. This is consistent with the regional response modeled by *Keen and Glenn* [1995]. Typical nor'easter storm transport events observed at the LEO site have an alongshore component to the south and a cross-shore component toward the coast [*Styles*, 1998; *Styles and Glenn*, 2005]. *Styles* [1998] suggests that the onshore component is steered by the local topography. Since the event seen during Floyd has an offshore component, it appears that the direction and possibly the duration of the tropical storm forcing is sufficient to overcome the local steering effects of topography. Unlike nor'easters in which the winds are from the northeast, the winds immediately following Floyd had a strong offshore component (Figure 3) that steers the alongshore flow slightly offshore (Figure 10), leading to net transport away from the coast.

[36] The shallow well-mixed response to the passing of Tropical Storm Floyd is a short episodic event. The effect of the storm perturbs the current structure for about 48 hours before the seasonal climatology returns. While there is energy in the near-inertial band, it is not the typical clockwise rotation seen with baroclinic responses in a deeper stratified ocean. Instead the oscillating sea surface slope associated with the fast moving storm and the increased influence of the bottom stress drives an alongshore current that accelerates to the north and south with the changing sea surface. Following the storm, freshwater stratifies the water column, shifting the response from a single layer to a two-layer system. Through the entire event the energy put into the system by the storm is quickly dissipated by bottom friction. The results presented here show that the response of the inner shelf to a passing tropical storm is much shorter than that seen in deeper more

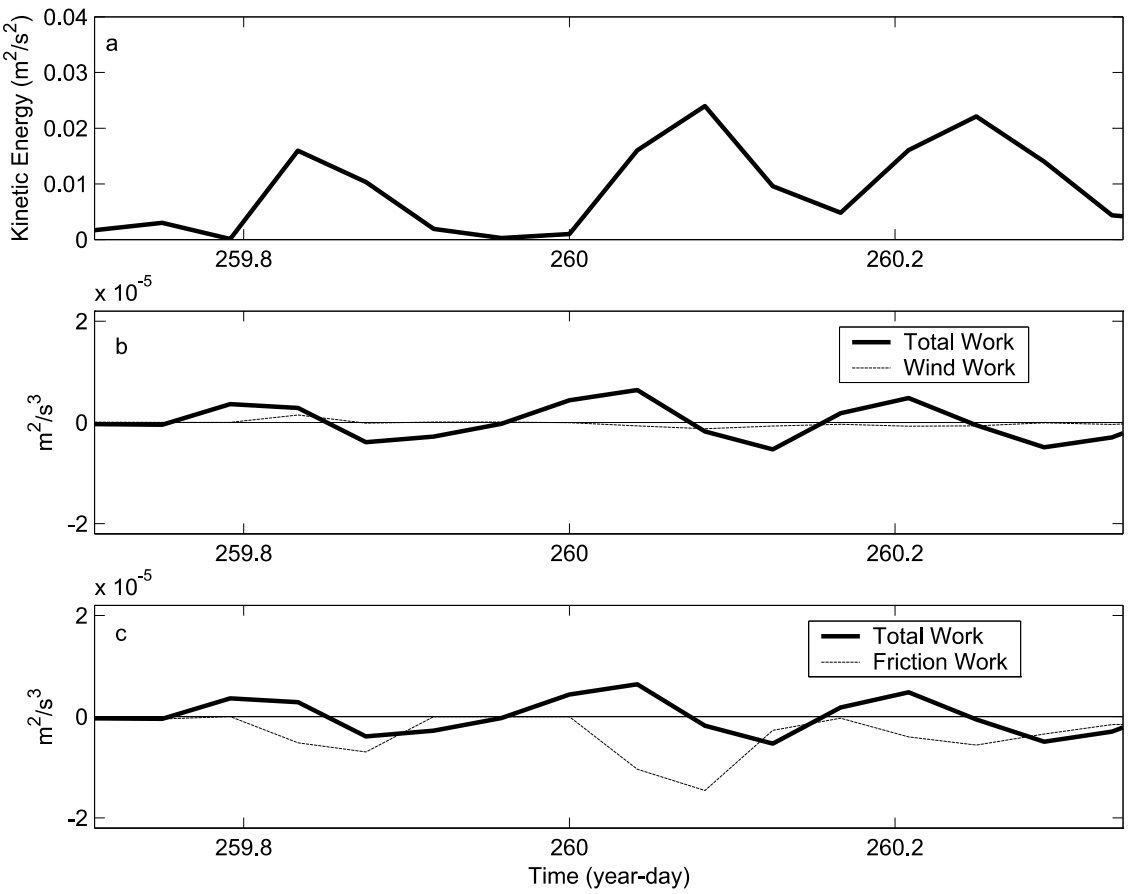

Figure 16. Alongshore (a) kinetic energy, (b) work done by the wind, and (c) work done by bottom friction. The total work is quantified as the change in kinetic energy (equation (8)).

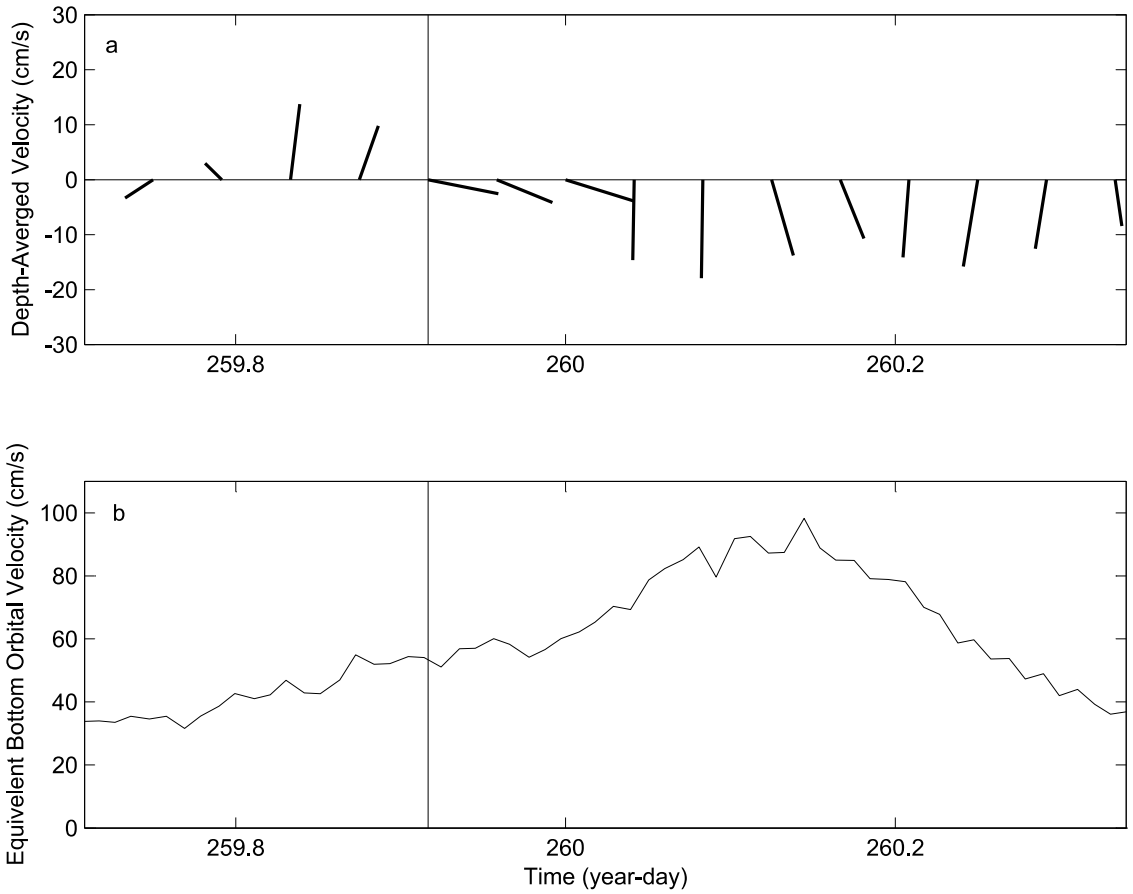

Figure 17. (a) Depth-averaged currents and (b) equivalent bottom wave orbital velocities associated with Tropical Storm Floyd. The vertical line indicates the passage of the storm eye.

stratified domains. This response is a largely barotropic, setup by the storm surge and local winds. The oscillating alongshore flow is an immediate response to the direct storm forcing that quickly dissipates. The larger-scale northward flow, setup by the cross-shore winds is then maintained for a day after the storm by the continued offshore winds.

[37] Timing of the storm surge occurs during the unstratified initial response when bottom friction is important to the force balance. Thus storm surge models should contain accurate representations of the bottom friction that include the influence of the waves.

References

Barrick, D. E., and B. J. Lipa (1986), Correcting for distorted antenna patterns in CODAR ocean surface measurements, *IEEE J. Oceanic Eng*, *11*, 304–309.

Barrick, D. E., M. W. Evens, and B. L. Weber (1977), Ocean surface currents mapped by radar, *Science*, *198*, 138–144.

Brooks, D. A. (1983), The wake of Hurricane Allen in the western Gulf of Mexico, *J. Phys. Oceanogr.*, *13*, 117–129.

Chant, R. J. (2001), Evolution of near-inertial waves during an upwelling event on the New Jersey inner shelf, *J. Phys. Oceanogr.*, *31*, 746–763.

Dean, R. G., and R. A. Dalrymple (1991), Storm surge, in *Water Wave Mechanics for Engineers and Scientists*, edited by P. L. Liu, pp. 157–163, World Sci., Hackensack, N. J.

Fairall, C. W., E. F. Bradley, D. P. Rogers, J. B. Edson, and G. S. Young (1996), Bulk parameterization of air-sea fluxes for TOGA COARE, *J. Geophys. Res.*, *101*, 3747–3764.

Fandry, C. B., and R. K. Steedman (1994), Modelling the dynamics of the transient, barotropic response of continental shelf waters to tropical cyclones, *Cont. Shelf Res.*, *14*, 1723–1750.

Forristall, G. Z., R. C. Hamilton, and V. J. Cardone (1977), Continental shelf currents in Tropical Storm Delia: Observations and theory, *J. Phys. Oceanogr.*, *7*, 532–546.

Glenn, S. M., W. Boicourt, B. Parker, and T. D. Dickey (2000), Operational observation networks for ports, a large estuary and an open shelf, *Oceanography*, *13*, 12–23.

Grassle, J. F., S. M. Glenn, and C. von Alt (1998), Ocean observing systems for marine habitats, paper presented at OCC '98, Mar. Technol. Soc., Baltimore, Md.

Keen, T. R., and S. M. Glenn (1995), A coupled hydrodynamic-bottom boundary layer model of storm and tidal flow in the Middle Atlantic Bight of North America, *J. Phys. Oceanogr.*, *25*, 391–406.

Keen, T. R., and S. M. Glenn (1999), Shallow water currents during Hurricane Andrew, *J. Geophys. Res.*, *104*, 23,443–23,458.

Kohut, J. T., and S. M. Glenn (2003), Improving HF radar surface current measurements with measured antenna beam patterns, *J. Atmos. Oceanic Technol.*, *20*, 1303–1316.

Kohut, J. T., S. M. Glenn, and R. J. Chant (2004), Seasonal current variability on the New Jersey inner shelf, *J. Geophys. Res.*, *109*, C07S07, doi:10.1029/2003JC001963.

Kundu, P. K. (1984), Generation of coastal inertial oscillations by time-varying wind, *J. Phys. Oceanogr.*, *14*, 1901–1913.

Kundu, P. K. (1986), A two-dimensional model of inertial oscillations generated by a propagating wind field, *J. Phys. Oceanogr.*, *16*, 1399–1411.

Mayer, D. A., H. O. Mofjeld, and K. D. Leaman (1981), Near-inertial waves observed on the outer shelf in the Middle Atlantic Bight in the wake of Hurricane Belle, *J. Phys. Oceanogr.*, *11*, 87–106.

Paduan, J. D., R. A. De Szoeke, and R. A. Weller (1989), Inertial oscillations in the upper ocean during the Mixed Layer Dynamics Experiment (MILDEX), *J. Geophys. Res.*, *94*, 4835–4842.

Price, J. F., T. B. Sanford, and G. Z. Forristall (1994), Forced stage response to a moving hurricane, *J. Phys Oceanogr.*, *24*, 233–260.

Schofield, O., T. Bergmann, W. P. Bissett, F. Grassle, D. Haidvogel, J. Kohut, M. Moline, and S. Glenn (2001), The long term ecosystem observatory: An integrated coastal observatory, *IEEE J. Oceanic Eng.*, *27*, 146–154.

Shay, L. K., and S. W. Chang (1997), Free surface effects on the near-inertial ocean current response to a hurricane: A revisit, *J. Phys. Oceanogr.*, *27*, 23–39.

Shay, L. K., and R. L. Elsberry (1987), Near-inertial ocean current response to Hurricane Frederic, *J. Phys. Oceanogr.*, *17*, 1249–1269.

Shay, L. K., S. W. Chang, and R. L. Elsberry (1990), Free surface effects on the near-inertial ocean current response to a hurricane, *J. Phys. Oceanogr.*, *20*, 1405–1424.

Styles, R. (1998), A continental shelf bottom boundary layer model: Development, calibration, and applications to sediment transport in the Middle Atlantic Bight, Ph.D. dissertation, 261 pp., Rutgers–State Univ. of N. J., New Brunswick.

Styles, R., and S. M. Glenn (2002), Modeling bottom roughness in the presence of wave-generated ripples, *J. Geophys. Res.*, *107*(C8), 3110, doi:10.1029/2001JC000864.

Styles, R., and S. M. Glenn (2005), Long-term sediment mobilization at a sandy inner shelf site, LEO-15, *J. Geophys. Res.*, *110*, C04S90, doi:10.1029/2003JC002175.

Valle-Levinson, A., K. Wong, and K. T. Bosley (2002), Response of the lower Chesapeake Bay to forcing from Hurricane Floyd, *Cont. Shelf Res.*, *22*, 1715–1729.

S. M. Glenn and J. T. Kohut, Institute of Marine and Coastal Sciences, Rutgers–State University of New Jersey, 71 Dudley Road, New Brunswick, NJ 08901, USA. (kohut@imcs.rutgers.edu)

J. D. Paduan, Code OC/Pd, Naval Postgraduate School, Monterey, CA 93943, USA.